# Exploration of the Amino Acid Metabolic Signature in Anthracycline-induced Cardiotoxicity Using an Optimized Targeted Metabolomics Approach Based on UPLC-MS/MS

**Wendi Li**
Peking University People's Hospital https://orcid.org/0000-0003-2093-8410
**Shanshan Li**
Peking University People's Hospital
**Zhenju Cao**
Peking University People's Hospital
**Yi Sun**
Peking University People's Hospital
**Wei Qiu**
Capital Medical University Affiliated Beijing Friendship Hospital
**Mei Jia**
Peking University People's Hospital
**Ming Su** ( suming@bjmu.edu.cn )
Peking University People's Hospital https://orcid.org/0000-0002-0252-7936

**Primary research**

**Keywords:** Targeted metabolomics, Anthracycline-induced cardiotoxicity, Amino acid metabolism, Signature

**Posted Date:** November 2nd, 2021

**DOI:** https://doi.org/10.21203/rs.3.rs-1018930/v1

# Abstract

**Background:** Although anthracyclines improve the long-term survival rate of patients with cancer, severe and irreversible myocardial damage limits their clinical application. Amino acids (AAs) play critical roles in protein synthesis, energy generation, and metabolism, as well as maintenance of the normal structure of cardiomyocytes. Conversely, AA metabolism in cardiomyocytes can be altered under pathological conditions. Therefore, exploring the AA metabolic signature in anthracycline-induced cardiotoxicity (AIC) is important for identifying novel mechanisms.

**Methods:** We established mouse and cellular models of Adriamycin (ADR)-induced cardiac injury. Using a targeted AA metabolomics approach based on ultra-performance lipid chromatography–tandem mass spectrometry (UPLC-MS/MS), we quantified more than 120 AA metabolites through derivatization-assisted sensitivity enhancement with 5-aminoisoquinolyl-*N*-hydroxysuccinimidyl carbamate (5-AIQC). The AA metabolic signatures in the sera of AIC mice and supernatant samples of ADR-treated H9c2 cardiomyocytes were analyzed.

**Results:** The levels of 14 AA metabolites were altered in ADR-treated mice ($p < 0.05$). l-2-aminoadipic acid (2-AA) was one of the most suppressed metabolites in AIC. Pre-treatment with 2-AA failed to alter ADR-induced cardiac function impairment, but it exacerbated the ADR-induced decrease of left ventricular anterior wall thickness, indicating that 2-AA might contribute to AIC. Via bioinformatics analysis, we identified nine differential AA metabolites in mice, namely l-glutamic acid, l-lysine, l-serine, l-tryptophan, l-methionine, l-histidine, l-asparagine, l-tyrosine, and *O*-phosphorylethanolamine, and five differential AA metabolites in ADR-treated H9c2 cardiomyocytes, specifically l-tyrosine, l-alanine, l-glutamine, l-serine, and l-glutamic acid. Three AAs with increased levels (l-glutamate, l-serine, and l-tyrosine) overlapped in the two models, suggesting a possible mechanism of AA metabolic impairment during AIC. The metabolic pathways perturbed by AIC involved aminoacyl-tRNA biosynthesis and alanine, aspartate, and glutamate metabolism.

**Conclusions:** These data indicate that a targeted AA metabolomics approach based on UPLC-MS/MS can be used to explore the AA metabolic signature and identify novel mechanisms of AIC, which may provide new clues for the prevention and treatment of this condition in the early clinical stage.


# Background

Anthracyclines feature a tetracyclic ring structure (aglycone) attached by sugars or amino sugars through glycosidic bonds, and anthracyclines differ in their ligands or sugars [1]. Anthracyclines remain the cornerstones of chemotherapy for malignancies including lymphoma, sarcoma, breast cancer, and pediatric leukemia because of their significant anti-cancer effects. According to available data, anthracyclines are used to treat approximately 30% of breast cancers, up to 70% of lymphomas in older adults, and 60% of pediatric cancers [2]. Although anthracyclines improve the long-term survival rate of patients with cancer, they cause severe and irreversible myocardial damage, thereby limiting their clinical

application [3]. The observation of a relationship between the anthracycline dose and cardiovascular side effects can be traced back four decades [4]. When the cumulative dose of doxorubicin exceeds 250–300 mg/m$^2$, the risk of cardiotoxicity rises dramatically [5]. Cardinale *et al.* found that anthracycline-induced cardiotoxicity (AIC) occurred in 9% of adults, and the incidence of AIC is highest (98%) during the first year after the completion of chemotherapy [6]. To date, anthracyclines remain the major cause of chemotherapy-induced cardiotoxicity [7, 8]. AIC, the mechanism of which has not been fully clarified, is a broad term encompassing both changes in resting cardiac parameters and dynamic functional assessments of the cardiovascular system such as diminished left ventricular ejection fraction, cardiac cell and structural damage, conduction abnormalities, vascular abnormalities, and other adverse effects that perturb normal cardiac function. Therefore, identifying new insights into the mechanism of AIC is critical for clinical prevention and treatment.

Amino acids (AAs) are essential for protein synthesis and the maintenance of normal heart structure, but they also can be catabolized as substrates for energy generation [9]. Therefore, an imbalance of AA metabolism induces myocardial contractile dysfunction and eventually heart failure [10, 11]. Murashige *et al*. measured more than 270 metabolites using liquid chromatography–mass spectrometry (MS) in patients with heart failure and reported a high level of AA secretion from the heart, indicating that AA metabolic disorder may contribute to cardiac injury [12]. In comparison with glucose and fatty acids as metabolic fuels for the heart, the role of AA metabolic pathways in the heart has received little attention. Emerging evidence suggests that AAs are closely related to AIC [13, 14], and it is of great significance to explore the role of AA metabolism in AIC. However, it is unclear whether AA metabolism is altered in AIC. In the present study, we established Adriamycin (ADR)-induced cardiac injury models. Using an optimized targeted AA metabolomics method based on ultra-performance liquid chromatography–tandem MS (UPLC-MS/MS), we obtained the AA metabolic signature of AIC.

## Materials And Methods

# Chemicals and reagents

Doxorubicin hydrochloride (ADR) was obtained from Solarbio (Beijing, China). l-2-aminoadipic acid (2-AA) was purchased from Aladdin (Shanghai, China). HPLC-grade formic acid, acetonitrile, and methanol were purchased from Thermo Fisher Scientific (Waltham, MA, USA). AR-grade $K_2HPO_4{\cdot}3H_2O$ and $NaH_2PO_4{\cdot}2H_2O$ were purchased from Sinopharm Chemical Reagent Co., Ltd. (China). AR-grade boric acid, *N*-ethylmaleimide (NEM), 4-tert-butylbenzenethiol (tBBT), dimethyl sulfoxide (DMSO), 5-aminoisoquinoline (5-AIQ), *N*,*N*-disuccinimidyl carbonate (DSC), ascorbic acid (Vc), ethylenediaminetetraacetic acid (EDTA), and phosphine hydrochloride (TCEP) were purchased from Sigma-Aldrich (St. Louis, MO, USA). The 126 amino analyte standards were purchased from Sigma-Aldrich and J&K Scientific (China). 5-Aminoisoquinolyl-*N*-hydroxysuccinimidyl carbamate (5-AIQC) for tagging amino groups was synthesized via the drop-wise addition of 5-AIQ solution (2 mmol in 50 mL ACN) to DSC solution (3 mmol in 40 mL ACN) over approximately 2 h at ambient temperature with

magnetic stirring. After further stirring for 24 h and removal of acetonitrile by rotary evaporation, 5-AIQC was obtained as crystals from the concentrated solution through filtration (650 mg, 82% yield). Phosphate buffer and borate buffer were prepared in a normal manner with their pH adjusted to 7.0 and 8.8, respectively, using sodium hydroxide solution. Phosphate buffer (0.1 M) contained 10 mM Vc and 10 mM EDTA, whereas borate buffer (0.2 M) contained 20 mM TCEP and 1 mM Vc. Cell Counting Kit-8 (CCK-8) was purchased from Dojindo (Kumamoto, Japan).

# Animal experiments

All animal protocols were approved by the Ethics Committee of Peking University People's Hospital (No. 2018PHC051). Six-to-eight-week-old male C57BL/6J mice were maintained on a 12-h/12-h light/dark cycle and permitted free access to food and water. Sixteen mice were weighed and randomly allocated to the ADR (n = 8) and control groups (n = 8); however, one mouse in the ADR group accidentally died during echocardiography, and it was excluded from the study. The AIC model was constructed as previously described [15]. In brief, mice in the ADR group were intraperitoneally injected with 15 mg/kg ADR on the first day of the experiment. An equal volume of normal saline was injected into the mice of the control group. For studies exploring the effects of 2-AA on ADR-treated mice, 32 mice were divided into four groups: control group, control + 2-AA group, ADR group, and ADR + 2-AA group (n = 8 per group). The mice treated with 2-AA were fed 500 mg/kg/day 2-AA, which was equivalent to a starting dose of 12.03 ± 0.30 mM, for 1 week before ADR injection. After ADR treatment, the mice were fed 2-AA for another week. Pre-weighed food and water were placed each cage. Food and water intake were monitored every day. Echocardiography was performed to determine the cardiac structure and function on the sixth day of the experiment. At least three measurements were conducted, and the values were averaged for each parameter. All mice were fasted for 12 h prior to subsequently sacrificed, and the serum samples were collected. In order to ensure that the collected tissues uncontaminated by chemical agents, we used cervical dislocation method for euthanasia. The animal experiments personnel have been professionally trained and certified by Beijing Association on Laboratory Animal Care (No. 1119112500107).

# Establishment of the ADR-induced H9c2 cell injury model

H9c2 (National Infrastructure of Cell Line Resource, Beijing, China) cells were cultured in Dulbecco's modified Eagle's medium (DMEM, Hyclone) containing 10% fetal bovine serum (FBS, BioInd, Israel) in a 37°C humidified atmosphere containing 5% $CO_2$ and 95% $O_2$. The cells were seeded onto 12-well plates at a density of $5 \times 10^5$ cells/mL for 24 h before the addition of ADR. H9c2 cells were treated with 1 μM ADR for 24 h, and cells treated with an equal volume of normal saline were used as a control. There were six parallel wells in each group. After treatment, the conditioned medium samples were collected and centrifuged at 12,000 rpm to remove the precipitates, and the supernatants were immediately stored at −80°C.

# CCK-8 assay

The viability of H9c2 cells after ADR treatment at concentrations of 0.5, 1, 2, 4, 8, and 16 μM was detected using the CCK-8 assay. H9c2 cells were seeded ($5 \times 10^3$ cells/mL) into 96-well plates and incubated with

various concentrations of ADR for 24 h at 37°C (0 μM used as a control). Subsequently, 10 μL of CCK-8 reagent were added to each well according to the manufacturer's protocol and incubated for 2 h at 37°C. The absorbance of each well at 450 nm was measured using a microplate reader, and the relative viabilities were analyzed.

# UPLC-MS/MS analysis

Serum samples (20 μL) or conditioned medium samples (20 μL) were each mixed with 60 μL of pre-cooled methanol for protein precipitation. Samples were vortexed and centrifuged at 12,000 rpm for 10 min at 4°C. Then, ten μL of the supernatant were vortex-mixed with 10 μL of NEM solution (20 mM) in phosphate buffer for 1 min. Ten microliters of tBBT solution (0.23 M in DMSO) were added followed the addition of 87.5 μL of borate buffer. After vortexing and standing for 2 min, 33 μL of 5-AIQC solution were then added, followed by incubation at 55°C for 10 min. The mixture was cooled to ambient temperature and mixed with 2 μL of formic acid, and the solution was filtered through a 0.22-μm membrane filter before UPLC-MS/MS analysis.

Quantitative detection of amino analytes was performed by UPLC-MS/MS using a previously reported optimized method [16]. The UPLC-MS/MS system consisted of an Agilent 1290 UPLC coupled to an Agilent 6470 triple quadrupole mass spectrometer equipped with an electrospray ionization (ESI) source (Agilent Technologies, USA). The 5-AIQC–tagged samples (1 μL) were individually injected into an UPLC column (Agilent ZORBAX RRHD Eclipse XDB C18 column, 2.1 × 100 mm, 1.8 μm particles) with its temperature set to 50°C. The mobile phase consisted of solvent A (water) and solvent B (methanol containing 0.1% formic acid), and the flow rate was 0.5 mL/min. An optimized gradient elution was performed using the following scheme: 1% B (0–2 min), 1–3.8% B (2–4 min), 3.8–14% B (4–7.3 min), 14–22% B (7.3–10.7 min), 22–24% B (10.7–14.7 min), 24–30% B (14.7–16 min), 30–60% B (16–16.3 min), 60–70% B (16.3–17.3 min), 70–95% B (17.3–17.31 min), and 95% B (17.31–20 min). ESI was performed in the positive ion mode under the following conditions: nebulizer pressure, 50 psi; sheath gas temperature, 350°C (flow rate, 10 L/min); dry gas temperature, 315°C (flow rate, 10 L/min); and capillary voltage, 4000 V. Multiple reaction monitoring was used for the quantification of screening fragment ions. Quality control samples were prepared using no fewer than 5% of the total number of samples divided into three parallel parts throughout the whole process of sample preparation, detection, and analysis.

# Data preprocessing and statistical analysis

Peak determination and peak area integration were performed using MassHunter Workstation software (Agilent, Version B.08.00). Standard curves were constructed by least-squares linear regression analysis using the peak area ratio of the derivatized individual standard against the nominal concentration of the calibrator. Quantification of samples was performed identically. Statistical analysis was performed using SPSS 22.0 software. AA levels were compared between the ADR and control groups using Student's *t*-test, and $p < 0.05$ denoted statistical significance. Multivariate statistical analysis was performed using Simca-P 14.1. Principal component analysis (PCA) was used to gain an overview of all samples and find possible outliers. Orthogonal partial least squares discriminant analysis (OPLS-DA) modeling was used

to screen differential metabolites that contributed significantly to the discrimination of samples from each group. The criteria for identifying significant differential metabolites were variable importance in projection (VIP) > 1.0 and $p < 0.05$ in the OPLS-DA model. Meanwhile, the relevant metabolic pathways were enriched by MetaboAnalyst 5.0 (http://www.metaboanalyst.ca), as well to discover the significant pathways in the two models.

## Results

# ADR induces cardiac injury in mice

To establish experimental AIC in mice, 15 mg/kg ADR was injected intraperitoneally [15]. Echocardiographic analysis was performed on the sixth day after ADR treatment. The representative echocardiographic images are presented in Fig. 1A. We found that ADR induced a significant decrease of the ejection fraction (EF%), demonstrating that the mouse model was successfully established. In addition, we observed that the left ventricular fractional shortening (LVFS) was significantly lower in the ADR group than in the control group, suggesting that ADR treatment impaired cardiac systolic function (Fig. 1B). The left ventricular posterior wall thickness at end diastole (LVPWd) and systole (LVPWs) and the left ventricular anterior wall thickness at end diastole (LVAWd) and systole (LVAWs) were remarkably lower in the ADR group than in the control group, indicating that cardiac structural remodeling was induced by ADR (Fig. 1B).

# Identification of differential AA metabolites in mice

AA profiles were obtained using validated and robust methodology, enabling the quantitation of 62 analytes from serum samples. In all analyzed samples, there were 51 detectable analytes. The concentrations of the remaining nine analytes were below the limit of quantitation (LOQ) or they exceeded the LOQ for some of the samples; thus, they were excluded from statistical analyses. The AA levels were compared between the ADR and control groups using Student's *t*-test (Supplementary Table S1). We identified 14 differential metabolites ($p < 0.01$) in mice, including 10 metabolites with increased levels (l-lysine, l-serine, 5-aminovaleric acid, l-asparagine, *O*-phosphorylethanolamine, l-glutamic acid, l-methionine, l-histidine, l-tyrosine, l-tryptophan) and 4 metabolites with decreased levels (ethanolamine, cystathionine, 2-AA, l-glutathione oxidized) (Fig. 2).

Among these differential metabolites, we found that the levels of 2-AA, an intermediate compound in lysine metabolism, were significantly decreased. Recently, 2-AA was identified as a biomarker of insulin resistance, obesity, and diabetes [17, 18]. To explore the role of 2-AA in AIC, mice were fed with 2-AA daily for 1 week prior to ADR treatment. Data from echocardiography revealed that ADR treatment caused significant decreases of EF%, FS%, LVAWs, and LVPWs (Fig. 3B). However, EF%, FS%, and LVPW were not altered by 2-AA treatment in AIC mice, whereas LVAWs and LVAWd were lower in the ADR + 2-AA group than in the ADR group, suggesting that 2-AA treatment exacerbates AIC in mice.

# Bioinformatic analysis of AA metabolites in mice

We then processed the 51 analyzed metabolites using PCA to obtain an overview of the data and identify potential severe outliers between the ADR and control groups regarding the metabolic profiles (Fig. 4A; principal component 1 [PC1], 49.9%; PC2, 18.3%). The distribution of metabolites in the control group was more compact, whereas that in the ADR group was more dispersed. However, the PCA score plot failed to reveal clear separation between the analyzed groups. The results demonstrated that the PCA-X model could not completely distinguish the ADR and control groups. A supervised OPLS-DA model was then established to acquire clustering information and differential metabolites to differentiate the ADR and control groups. The variables significant at VIP > 1.0 and $p < 0.05$ in the OPLS-DA model were considered as biomarker candidates. We used the parameters R2 and Q2 to assess the fitness and prediction capabilities of the OPLS-DA model, respectively. The OPLS-DA model resulted in two predictive components with R2X (cum) = 0.742, R2Y (cum) = 0.931, Q2 (cum) = 0.776. Meanwhile, coefficient variability analysis of variance (CV-ANOVA) and permutation testing were further used to validate the OPLS-DA model. The *p* value of CV-ANOVA in this established model was 0.025, and the plot of permutation testing with 200 permutations is presented in Fig. S1A. The OPLS-DA score plots of serum samples are presented in Fig. 4B, in which clear separation between the two groups is observed. The result suggests that the model has good practicability and predictability, and the separation reveals fundamental metabolic differences between the two groups. The plot of the predictive VIP values is presented in Fig. S2A. Metabolites in the serum samples that satisfied both VIP > 1.0 and $p < 0.05$ are listed in Table 1. Nine metabolites including l-glutamic acid, l-lysine, l-serine, l-tryptophan, l-methionine, l-histidine, l-asparagine, l-tyrosine, and *O*-phosphorylethanolamine comprised the signature of AIC in ADR-treated mice. Furthermore, MetaboAnalyst 5.0 was applied to analyze the data of differential metabolites to find the potential metabolic pathways based on Kyoto Encyclopedia of Genes and Genomes database, and the result is presented in Fig. 4C. Multiple metabolic pathways were perturbed by AIC, especially d-glutamine and d-glutamate metabolism; histidine metabolism; alanine, aspartate, and glutamate metabolism; aminoacyl-tRNA biosynthesis; and arginine biosynthesis. Detailed pathway results are summarized in Table S2.

**Table 1**

Amino acid metabolic signature of Adriamycin-induced cardiotoxicity in mice

| Amino Acid | VIP value | *p* value |
|---|---|---|
| l -Glutamic acid | 3.70606 | $p<0.0001$ |
| l -Lysine | 2.87705 | 0.039 |
| l -Serine | 1.82098 | 0.023 |
| l -Tryptophan | 1.80749 | 0.024 |
| l -Methionine | 1.57079 | 0.003 |
| l -Histidine | 1.36099 | 0.010 |
| l -Asparagine | 1.16729 | 0.012 |
| l -Tyrosine | 1.1004 | 0.028 |
| *O*-Phosphorylethanolamine | 1.08842 | $p<0.0001$ |

Variable importance for projection (VIP) from the orthogonal partial least squares discriminant analysis model constructed with the control and model groups.

Considering that the *in vivo* model might reflect the global AA metabolic status, we established an *in vitro* model using ADR-treated cardiomyocytes to specifically focus on the AA metabolic signature in AIC. H9c2 cells were treated with ADR at various concentrations for 24 h. Data from the CCK-8 assay indicated that treating H9c2 cells with 1 μM ADR significantly induced cytotoxicity (Fig. 5). Therefore, this concentration was selected for the AA metabolism study. Using UPLC-MS/MS, we identified 15 AA metabolites with significantly different levels among 44 detected metabolites in the conditioned medium of ADR-treated H9c2 cells (Table S3). The levels of 10 AA metabolites (hypotaurine, d-homoserine, 2-AA, ethanolamine, taurine, l-asparagine, l-glutamic acid, l-serine, l-glutamine, l-tyrosine) were increased in the ADR group, whereas those of five AA metabolites (cadaverine, l-homocystine, l-aspartic acid, l-ornithine, l-alanine) were decreased (Fig. 6). The 44 analyzed metabolites were processed by PCA to characterize the metabolic profile of the cellular model (PC1, 60.5%; PC2, 24.6%, Fig. 7A). The PCA score plot revealed clear separation between the analyzed data groups, indicating that two groups had different metabolic profiles.

Supervised OPLS-DA was also performed within the *in vitro* model. The OPLS-DA score plots of culture medium supernatant samples are presented in Fig. 7B, and the plot of the predictive VIP values is presented in Fig. S2B. The OPLS-DA model revealed clear separation between the analyzed data groups, indicating that significant changes of AA metabolism occurred after ADR treatment. Five metabolites (l-tyrosine, l-alanine, l-glutamine, l-serine, l-glutamic acid) satisfying both VIP > 1.0 and $p < 0.05$ were identified as the signature of AIC in the cellular injury model (Table 2). Five important pathways including phenylalanine, tyrosine, and tryptophan biosynthesis; alanine, aspartate, and glutamate metabolism; glycine, serine, and threonine metabolism; aminoacyl-tRNA biosynthesis; and tyrosine metabolism were perturbed in the *in vitro* AIC model (Fig. 7C and Table S4).

**Table 2**

Amino acid metabolic signature in Adriamycin-induced H9c2 cell injury models

| Amino Acid | VIP value | *p* value |
|---|---|---|
| l -Tyrosine | 3.63705 | *p*<0.0001 |
| l -Alanine | 2.76496 | *p*<0.0001 |
| l -Glutamine | 2.60996 | 0.025 |
| l -Serine | 2.54653 | *p*<0.0001 |
| l -Glutamic acid | 2.11724 | *p*<0.0001 |

# Pathway analysis

Via an overlap analysis, we found that the levels of three AAs, namely l-glutamate, l-serine, and L-tyrosine, were increased in both the *in vivo* and *in vitro* models (Fig. 8A), suggesting AA utilization impairment in AIC. Furthermore, we found the aminoacyl-tRNA biosynthesis and alanine, aspartate, and glutamate metabolism were both involved in the two models (Fig. 8B), suggesting the two pathways might be associated with AIC.

# Discussion

The incidence of cancer-related diseases has increased without a consequent rise in cancer-related mortality, which is attributable to the remarkable progress in cancer treatment [19]. With this change, people have increasingly recognized the importance of the adverse effects of cancer therapies, including chemotherapy-induced cardiotoxicity. Anthracyclines remain the cornerstones of cancer chemotherapy. Unfortunately, severe and irreversible myocardial damage limits their clinical application. Despite more than five decades of research, the mechanism underlying AIC is not completely understood [4]. In the present study, we established ADR-induced cardiac injury models. Using an optimized targeted AA metabolomics method based on UPLC-MS/MS, we analyzed the changes of AA metabolites in AIC.

In the present study, a new parameter-optimized UPLC-MS/MS method based on 5-AIQC derivatization-assisted sensitivity enhancement for the simultaneous quantification of amino-containing metabolites was developed. Using an NEM click reaction followed by the addition of anti-oxidants (TCEP and Vc), our method enabled the simultaneous quantification of amino analytes in a one-pot manner (and in a single run). This 5-AIQC–based method had high sensitivity for an extensive array of analytes including 20 proteinogenic AA, more than 10 modified AAs, more than 50 non-proteinogenic AAs, more than 20 sulfur-containing analytes, more than 10 monoamine neurotransmitters (e.g., catecholamines), a variety of small peptides, and aliphatic and aromatic amines. This method enabled the simultaneous quantification of more than 100 important functional metabolites involved in more than 20 metabolic pathways such as

protein biosynthesis/degradation; catecholamine, arginine, and glutathione biosynthesis; and homocysteine and taurine metabolism. Therefore, the present method offers many advantages for metabolomic analysis, such as wide metabolite coverage, excellent precision, accuracy, linearity repeatability, and capability in biomarker discovery, making it useful for both basic and clinical metabolic research [16].

“Omics” technologies such as proteomics, metabolomics, and genomics have emerged as promising tools for discovering novel biomarkers associated with cardiotoxicity [20–23]. These techniques have the potential to uncover novel pathways and mechanisms of AIC. Among these modern techniques, metabolomics appears extremely promising for biomarker research because it can reflect changes in endogenous substances in different physiological or pathological states. Untargeted metabolomics fails to provide information about the absolute concentration of analyzed compounds, and it is limited by unsatisfactory repeatability and a requirement for complex data processing, making it difficult to use this strategy in clinical practice. Instead, targeted strategies use specific and optimized sample extraction techniques customized according to the physiochemical properties of the analytes of interest to achieve high sensitivity, high specificity. and excellent quantification ability [24].

AA metabolites, as the most important basic substances in the life movement of organisms, participate in various energy and substance metabolic pathways. In the present study, significant changes in AA analytes were identified as signatures in AIC models based on targeted AA metabolomic analysis. Regarding the AA metabolite profiling, we found that the levels of most of the metabolites were increased in the ADR groups, implying that prominent metabolite accumulation may occur in AIC. A metabolomic study based on gas chromatography-MS identified 21 metabolites in an ADR-induced toxicity rat model and found an upward trend of many AAs [25]. Another metabolomic analysis reported that the levels of many AAs were significantly increased in the heart tissues and plasma of ADR-treated B6C3F1 mice [26]. Sansbury *et al.* also reported extensive and pervasive increases in the levels of branched-chain AAs in the failing heart (both pressure-overloaded and infarcted mouse hearts) [27]. These findings indicated that the alteration of metabolism is a hallmark of dysfunctional hearts, and the disturbance of AA metabolism contributes to AIC [28–30].

In the present study, we identified 14 differential AA metabolites in the *in vivo* model and 15 metabolites in the *in vitro* model. Through OPLS-DA, the AA metabolic signatures of the two models were drawn to depict the effects of AIC on AA metabolism, and many of these individual metabolites have been reported to be associated with cardiac injury. Previous studies illustrated that alterations in the glutamate–glutamine cycle with an increase in glutamic acid levels and decrease in glutamine levels are associated with an unfavorable cardiometabolic status [31, 32]. l-tyrosine has been reported to be associated with heart failure [33]. In addition, tyrosine can be metabolized into p-cresyl sulfate, whereas tryptophan can be metabolized into indoxyl sulfate. These two metabolites contribute to adverse cardiac remodeling through their direct pro-fibrotic, pro-hypertrophic, and pro-inflammatory effects [34–36]. l-arginine is an essential AA with numerous functions. An earlier study linked l-arginine to mitochondrial function [37]. Another study reported that l-arginine can upregulate the serine biosynthesis pathway, which has been

demonstrated to fuel the tricarboxylic acid cycle and oxidative phosphorylation, and l-arginine can be converted into intermediates for energy generation [38]. Taurine is a sulfur-containing AA present abundantly in the heart, and it plays protective roles through the regulation of the intracellular $Ca^{2+}$ concentration and through its anti-oxidant, anti-inflammatory, anti-apoptosis, and membrane-stabilizing properties [39–42].

2-AA is a low-abundance AA previously described as an intermediate generated from circulating lysine by some unknown enzymatic pathway [43]. This relatively uncommon amino acid has recently attracted increasing attention because of its possible role as a modulator of glucose homeostasis in humans. A previous study suggested that 2-AA is a marker of diabetes risk using an untargeted metabolomics approach [18]. Previous studies of 2-AA in cardiac function are limited. Recently, Ganesh and colleagues found that 2-AA was involved in metabolic reprogramming in acute and chronic heart failure using a targeted metabolomics approach [44]. In our established *in vivo* and *in vitro* AIC models, we also found that the levels of 2-AA were different between the ADR and control groups. However, our data illustrated that 2-AA supplementation failed to improve or exacerbate AIC in mice, demonstrating that this AA does not participate in the progression of AIC despite changes in its levels.

Energetic metabolism in cardiomyocytes is a crucial feature of myocardial contractile function [45], and balanced AA metabolism is required. Using both *in vivo* and *in vitro* models, we found a dominant upward trend of AA metabolite levels under ADR treatment, indicating that abnormal AA metabolism associated with energetic utilization impairment or protein degradation may occur in AIC [12]. Through overlap pathway analysis, we identified significant differences in l-glutamate, l-serine, and L-tyrosine levels in the two models. Furthermore, we found that aminoacyl-tRNA biosynthesis and alanine, aspartate, and glutamate metabolism were involved in both the *in vitro* and *in vivo* models, suggesting that the two pathways are associated with AIC. A previous study revealed that aminoacyl-tRNA synthetases are involved in heart failure in humans and pathologic cardiac remodeling in mice. Aminoacyl-tRNA synthetases activate pro-fibrotic genes in cardiac fibroblasts in translational control and augment pathological cardiac remodeling [46]. Alanine, aspartate, and glutamate metabolism has been recognized as an important pathway associated with doxorubicin-induced nephropathy [47]. In any event, these results indicated an underlying AA disturbance exists in our ADR-induced cardiac injury model that is associated with AIC. Previous studies proposed that ADR-induced cardiotoxicity was associated with a variety of pathways and mechanisms, including reactive oxygen species formation, cardiomyocyte apoptosis, intracellular calcium dysregulation, and DNA damage [48–53]. Notably, our study explored AA metabolic signatures in AIC and provided valuable research directions concerning the mechanism of AIC.

# Conclusion

In conclusion, we explored the signature of AIC using targeted AA metabolomics techniques, which may provide new clues for the early and rapid diagnosis of AIC in patients under anthracycline therapy. Further studies using more specific methods are needed to reveal the exact mechanism in AIC involving key differential AA metabolites.

## Abbreviations

ADR, Adriamycin; AIC, anthracycline-induced cardiotoxicity; AA, amino acid; 2-AA, l-2-aminoadipic acid

## Declarations

# Acknowledgements

We thank Joe Barber Jr., PhD, for basic language editing of a draft of this manuscript.

# Funding

This study was supported by the National Natural Science Foundation of China (No. 81870196).

# Available of data and materials

The data that support the findings of this study are available from the corresponding author upon reasonable request.

# Ethics approval and consent to participate

Not applicable.

# Competing interests

The authors declare no competing interests associated with the manuscript.

# Consent for publication

Not applicable.

# Authors’ contributions

MJ, WQ and MS conceived and designed the study. WQ and MS provided financial supports. WL and SL performed most of the experiments, analyzed the data, and wrote the manuscript. ZC performed the cell experiments. YS assisted with performing the animal experiments. All authors have read and approved the final manuscript.

# Authors’ details

[1]Department of Clinical Laboratory, Peking University People’s Hospital, Beijing 100044, People’s Republic of China; [2]Department of Urology, Beijing Friendship Hospital, Capital Medical University, Beijing 100050, People's Republic of China.

# References

1. Mele D, Nardozza M, Spallarossa P, Frassoldati A, Tocchetti C, Cadeddu C, et al. Current views on anthracycline cardiotoxicity. Heart Fail Rev. 2016;21(5):621–34.
2. Sallustio B, Boddy A. Is there scope for better individualisation of anthracycline cancer chemotherapy? Br J Clin Pharmacol. 2021;87(2):295–305.
3. Sawicki K, Sala V, Prever L, Hirsch E, Ardehali H, Ghigo A. Preventing and Treating Anthracycline Cardiotoxicity: New Insights. Annu Rev Pharmacol Toxicol. 2021;61:309–32.
4. Middleman E, Luce J, Frei E. Clinical trials with adriamycin. Cancer. 1971;28(4):844–50.
5. Tantawy M, Pamittan F, Singh S, Gong Y. Epigenetic Changes Associated With Anthracycline-Induced Cardiotoxicity. Clin Transl Sci. 2021;14(1):36–46.
6. Cardinale D, Colombo A, Bacchiani G, Tedeschi I, Meroni C, Veglia F, et al. Early detection of anthracycline cardiotoxicity and improvement with heart failure therapy. Circulation. 2015;131(22):1981–8.
7. Lenneman C, Sawyer D. Cardio-Oncology: An Update on Cardiotoxicity of Cancer-Related Treatment. Circ Res. 2016;118(6):1008–20.
8. Mudd T, Khalid M, Guddati A. Cardiotoxicity of chemotherapy and targeted agents. Am J Cancer Res. 2021;11(4):1132–47.
9. Miyajima M. Amino acids: key sources for immunometabolites and immunotransmitters. Int Immunol. 2020;32(7):435–46.
10. De Jong K, Lopaschuk G. Complex Energy Metabolic Changes in Heart Failure With Preserved Ejection Fraction and Heart Failure With Reduced Ejection Fraction. Can J Cardiol. 2017;33(7):860–71.
11. Du X, You H, Li Y, Wang Y, Hui P, Qiao B, et al. Relationships between circulating branched chain amino acid concentrations and risk of adverse cardiovascular events in patients with STEMI treated with PCI. Sci Rep. 2018;8(1):15809.
12. Murashige D, Jang C, Neinast M, Edwards J, Cowan A, Hyman M, et al. Comprehensive quantification of fuel use by the failing and nonfailing human heart. Science. 2020;370(6514):364–8.
13. Tedesco L, Rossi F, Ragni M, Ruocco C, Brunetti D, Carruba M, et al. A Special Amino-Acid Formula Tailored to Boosting Cell Respiration Prevents Mitochondrial Dysfunction and Oxidative Stress Caused by Doxorubicin in Mouse Cardiomyocytes. Nutrients. 2020;12(2).

14. Xue H, Ren W, Denkinger M, Schlotzer E, Wischmeyer P. Nutrition Modulation of Cardiotoxicity and Anticancer Efficacy Related to Doxorubicin Chemotherapy by Glutamine and ω-3 Polyunsaturated Fatty Acids. JPEN J Parenter Enteral Nutr. 2016;40(1):52–66.
15. Shioji K, Kishimoto C, Nakamura H, Masutani H, Yuan Z, Oka S, et al. Overexpression of thioredoxin-1 in transgenic mice attenuates adriamycin-induced cardiotoxicity. Circulation. 2002;106(11):1403–9.
16. Wang J, Zhou L, Lei H, Hao F, Liu X, Wang Y, et al. Simultaneous Quantification of Amino Metabolites in Multiple Metabolic Pathways Using Ultra-High Performance Liquid Chromatography with Tandem-mass Spectrometry. Sci Rep. 2017;7(1):1423.
17. Lee H, Jang H, Kim W, Park K, Kim K, Park S, et al. 2-Aminoadipic acid (2-AAA) as a potential biomarker for insulin resistance in childhood obesity. Sci Rep. 2019;9(1):13610.
18. Wang T, Ngo D, Psychogios N, Dejam A, Larson M, Vasan R, et al. 2-Aminoadipic acid is a biomarker for diabetes risk. J Clin Invest. 2013;123(10):4309–17.
19. Herrmann J. Adverse cardiac effects of cancer therapies: cardiotoxicity and arrhythmia. Nat Rev Cardiol. 2020;17(8):474–502.
20. Serie D, Crook J, Necela B, Dockter T, Wang X, Asmann Y, et al. Genome-wide association study of cardiotoxicity in the NCCTG N9831 (Alliance) adjuvant trastuzumab trial. Pharmacogenet Genomics. 2017;27(10):378–85.
21. Wells Q, Veatch O, Fessel J, Joon A, Levinson R, Mosley J, et al. Genome-wide association and pathway analysis of left ventricular function after anthracycline exposure in adults. Pharmacogenet Genomics. 2017;27(7):247–54.
22. Ngo D, Sinha S, Shen D, Kuhn E, Keyes M, Shi X, et al. Aptamer-Based Proteomic Profiling Reveals Novel Candidate Biomarkers and Pathways in Cardiovascular Disease. Circulation. 2016;134(4):270–85.
23. Asnani A, Shi X, Farrell L, Lall R, Sebag I, Plana J, et al. Changes in Citric Acid Cycle and Nucleoside Metabolism Are Associated with Anthracycline Cardiotoxicity in Patients with Breast Cancer. J Cardiovasc Transl Res. 2020;13(3):349–56.
24. Zheng F, Zhao X, Zeng Z, Wang L, Lv W, Wang Q, et al. Development of a plasma pseudotargeted metabolomics method based on ultra-high-performance liquid chromatography-mass spectrometry. Nat Protoc. 2020;15(8):2519–37.
25. Geng C, Cui C, Wang C, Lu S, Zhang M, Chen D, et al. Systematic Evaluations of Doxorubicin-Induced Toxicity in Rats Based on Metabolomics. ACS omega. 2021;6(1):358–66.
26. Schnackenberg L, Pence L, Vijay V, Moland C, George N, Cao Z, et al. Early metabolomics changes in heart and plasma during chronic doxorubicin treatment in B6C3F1 mice. J Appl Toxicol. 2016;36(11):1486–95.
27. Sansbury B, DeMartino A, Xie Z, Brooks A, Brainard R, Watson L, et al. Metabolomic analysis of pressure-overloaded and infarcted mouse hearts. Circ Heart Fail. 2014;7(4):634–42.
28. Yuan Y, Fan S, Shu L, Huang W, Xie L, Bi C, et al. Exploration the Mechanism of Doxorubicin-Induced Heart Failure in Rats by Integration of Proteomics and Metabolomics Data. Front Pharmacol.

2020;11:600561.
29. Mamic P, Chaikijurajai T, Tang W. Gut microbiome - A potential mediator of pathogenesis in heart failure and its comorbidities: State-of-the-art review. J Mol Cell Cardiol. 2021;152:105–17.
30. Yi X, Zhu J, Zhang J, Gao Y, Chen Z, Lu S, et al. Investigation of the reverse effect of Danhong injection on doxorubicin-induced cardiotoxicity in H9c2 cells: Insight by LC-MS based non-targeted metabolomic analysis. J Pharm Biomed Anal. 2018;152:264–70.
31. Cheng S, Rhee E, Larson M, Lewis G, McCabe E, Shen D, et al. Metabolite profiling identifies pathways associated with metabolic risk in humans. Circulation. 2012;125(18):2222–31.
32. Papandreou C, Hernández-Alonso P, Bulló M, Ruiz-Canela M, Li J, Guasch-Ferré M, et al. High Plasma Glutamate and a Low Glutamine-to-Glutamate Ratio Are Associated with Increased Risk of Heart Failure but Not Atrial Fibrillation in the Prevención con Dieta Mediterránea (PREDIMED) Study. J Nutr. 2020;150(11):2882–9.
33. Cheng C, Liu M, Tang H, Cheng M, Wang C. Factors associated with elevated plasma phenylalanine in patients with heart failure. Amino acids. 2021;53(2):149–57.
34. Lekawanvijit S, Adrahtas A, Kelly D, Kompa A, Wang B, Krum H. Does indoxyl sulfate, a uraemic toxin, have direct effects on cardiac fibroblasts and myocytes? Eur Heart J. 2010;31(14):1771–9.
35. Lekawanvijit S, Kompa A, Manabe M, Wang B, Langham R, Nishijima F, et al. Chronic kidney disease-induced cardiac fibrosis is ameliorated by reducing circulating levels of a non-dialysable uremic toxin, indoxyl sulfate. PLoS One. 2012;7(7):e41281.
36. Fujii H, Nishijima F, Goto S, Sugano M, Yamato H, Kitazawa R, et al. Oral charcoal adsorbent (AST-120) prevents progression of cardiac damage in chronic kidney disease through suppression of oxidative stress. Nephrology, dialysis, transplantation. 2009;Nephrol Dial Transplant24(7):2089–95.
37. Geiger R, Rieckmann J, Wolf T, Basso C, Feng Y, Fuhrer T, et al. L-Arginine Modulates T Cell Metabolism and Enhances Survival and Anti-tumor Activity. Cell. 2016;167(3):829-42.e13.
38. Possemato R, Marks K, Shaul Y, Pacold M, Kim D, Birsoy K, et al. Functional genomics reveal that the serine synthesis pathway is essential in breast cancer. Nature. 2011;476(7360):346–50.
39. Ghosh J, Das J, Manna P, Sil P. Taurine prevents arsenic-induced cardiac oxidative stress and apoptotic damage: role of NF-kappa B, p38 and JNK MAPK pathway. Toxicol Appl Pharmacol. 2009;240(1):73–87.
40. Kim H, Jeon H, Kong H, Yang Y, Choi B, Kim Y, et al. A molecular mechanism for the anti-inflammatory effect of taurine-conjugated 5-aminosalicylic acid in inflamed colon. Mol Pharmacol. 2006;69(4):1405–12.
41. Schaffer S, Jong C, Ramila K, Azuma J. Physiological roles of taurine in heart and muscle. Journal of biomedical science. 2010:S2.
42. Samadi M, Haghi-Aminjan H, Sattari M, Hooshangi Shayesteh M, Bameri B, Armandeh M, et al. The role of taurine on chemotherapy-induced cardiotoxicity: A systematic review of non-clinical study. Life Sci. 2021;265:118813.

43. Lin H, Levison B, Buffa J, Huang Y, Fu X, Wang Z, et al. Myeloperoxidase-mediated protein lysine oxidation generates 2-aminoadipic acid and lysine nitrile in vivo. Free Radic Biol Med. 2017;104:20–31.
44. Halade G, Kain V, Tourki B, Jadapalli J. Lipoxygenase drives lipidomic and metabolic reprogramming in ischemic heart failure. Metabolism. 2019;96:22–32.
45. Neubauer S. The failing heart–an engine out of fuel. N Engl J Med. 2007;356(11):1140–51.
46. Wu J, Subbaiah K, Xie L, Jiang F, Khor E, Mickelsen D, et al. Glutamyl-Prolyl-tRNA Synthetase Regulates Proline-Rich Pro-Fibrotic Protein Synthesis During Cardiac Fibrosis. Circ Res. 2020;127(6):827–46.
47. Li A, Zhang W, Zhang L, Liu Y, Li K, Du G, et al. Elucidating the time-dependent changes in the urinary metabolome under doxorubicin-induced nephrotoxicity. Toxicol Lett. 2020;319:204–12.
48. Ichikawa Y, Ghanefar M, Bayeva M, Wu R, Khechaduri A, Naga Prasad S, et al. Cardiotoxicity of doxorubicin is mediated through mitochondrial iron accumulation. J Clin Invest. 2014;124(2):617–30.
49. Nitobe J, Yamaguchi S, Okuyama M, Nozaki N, Sata M, Miyamoto T, et al. Reactive oxygen species regulate FLICE inhibitory protein (FLIP) and susceptibility to Fas-mediated apoptosis in cardiac myocytes. Cardiovasc Res. 2003;57(1):119–28.
50. Arai M, Yoguchi A, Takizawa T, Yokoyama T, Kanda T, Kurabayashi M, et al. Mechanism of doxorubicin-induced inhibition of sarcoplasmic reticulum Ca(2+)-ATPase gene transcription. Circ Res. 2000;86(1):8–14.
51. Tewey K, Rowe T, Yang L, Halligan B, Liu L. Adriamycin-induced DNA damage mediated by mammalian DNA topoisomerase II. Science. 1984;226(4673):466–8.
52. Octavia Y, Tocchetti C, Gabrielson K, Janssens S, Crijns H, Moens A. Doxorubicin-induced cardiomyopathy: from molecular mechanisms to therapeutic strategies. Journal of molecular cellular cardiology. 2012;52(6):1213–25.
53. Henriksen P. Anthracycline cardiotoxicity: an update on mechanisms, monitoring and prevention. Heart. 2018;104(12):971–7.

# Figures

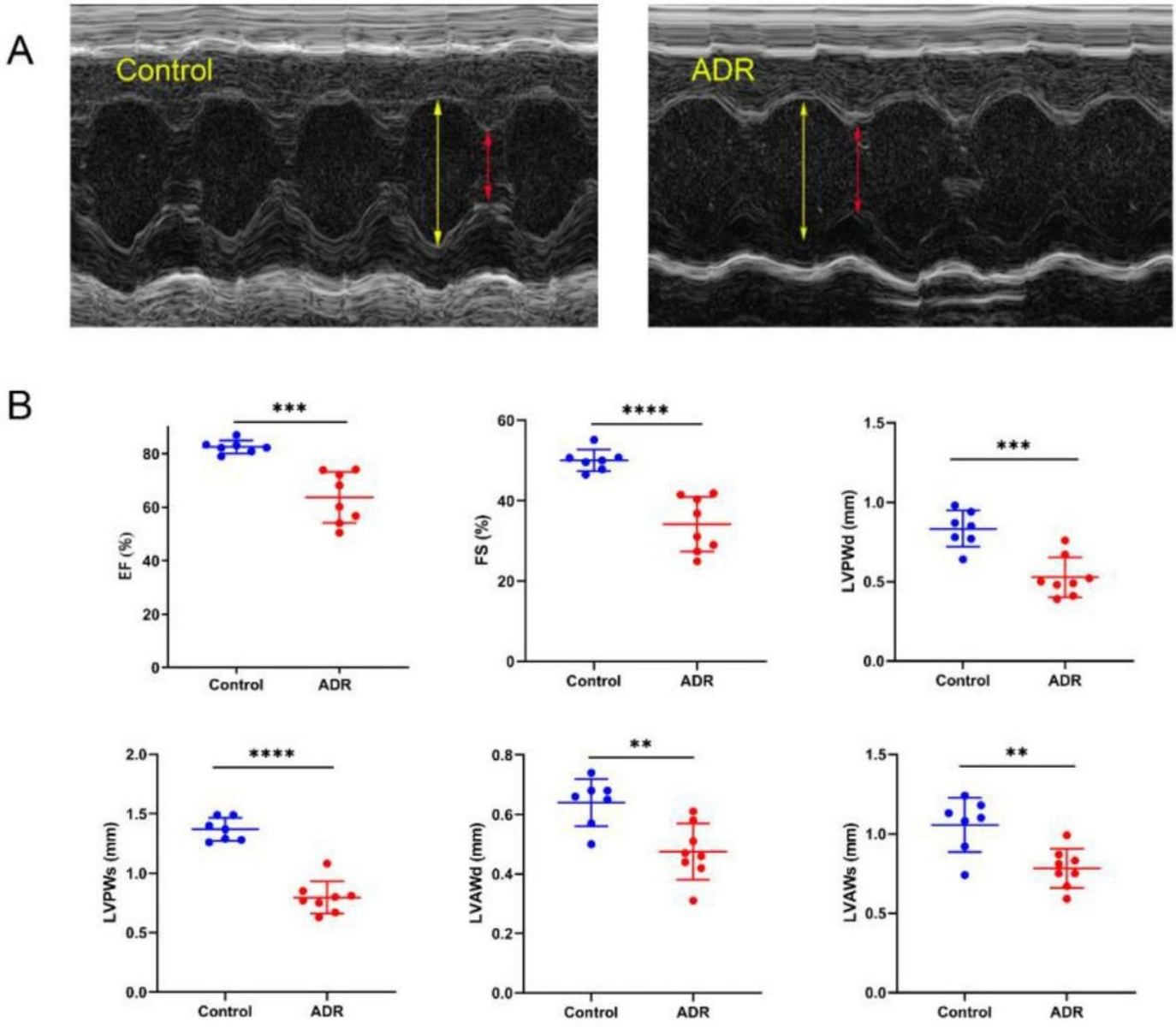


## Figure 1

Adriamycin (ADR) induces cardiac injury in mice. (A) Cardiac function and structure were detected by echocardiography, and representative images are presented. (B) The ejection fraction (EF%), fractional shortening (FS%), left ventricular posterior wall thickness at end diastole (LVPWd) and systole (LVPWs), and left ventricular anterior wall thickness at end diastole (LVAWd) and systole (LVAWs) were analyzed. Data are presented as the mean ± SD. ****$p < 0.0001$, ***$p < 0.001$, **$p < 0.01$, ns = not significant. ADR group (n = 8) vs. control group (n = 7).

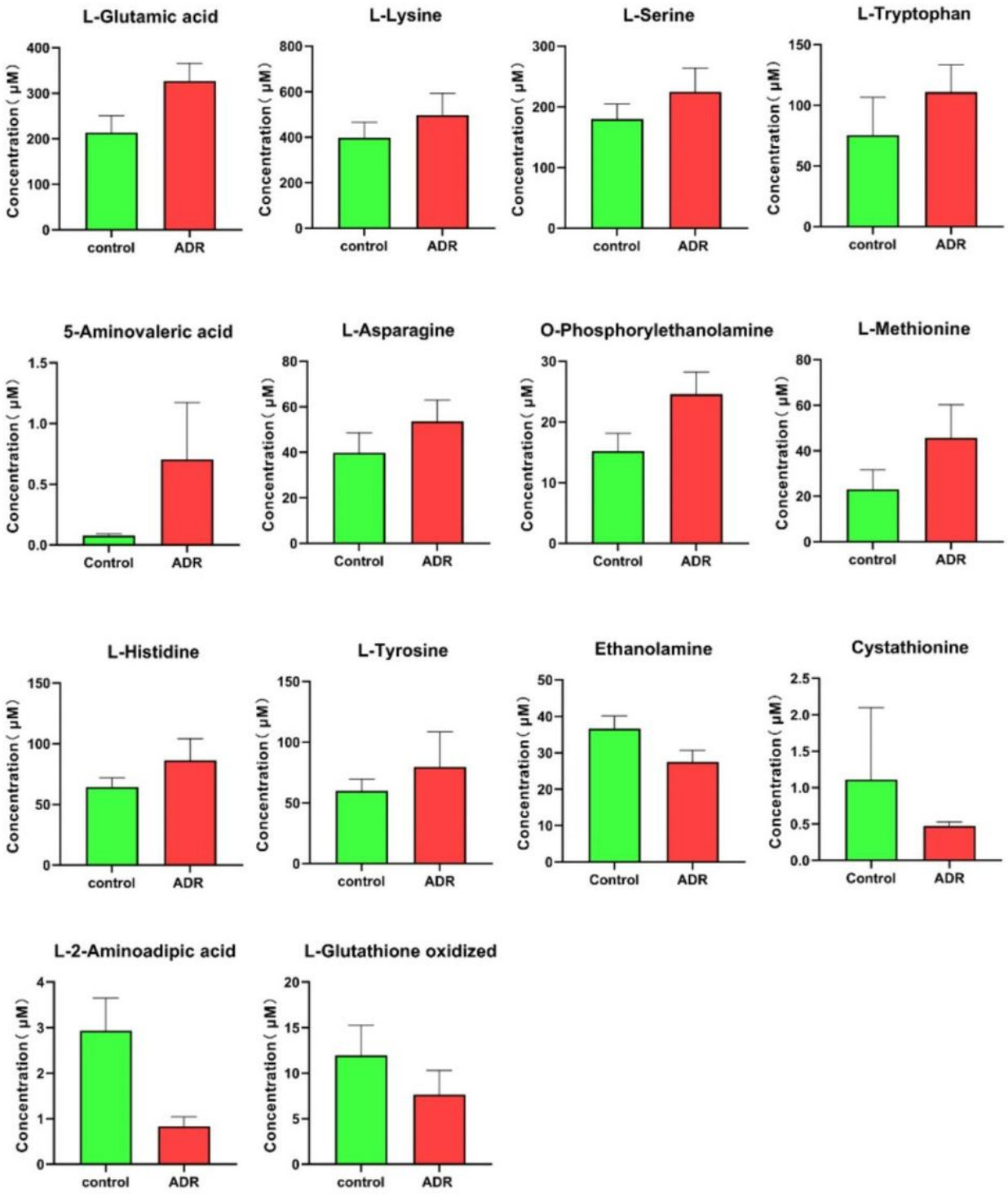


## Figure 2

Concentrations of 14 amino acid (AA) metabolites changed in mouse serum samples. Data are presented as the mean ± SD, and the levels of all 14 AA metabolites were significantly different ($p < 0.05$) between the ADR and ($n = 8$) control groups ($n = 7$).

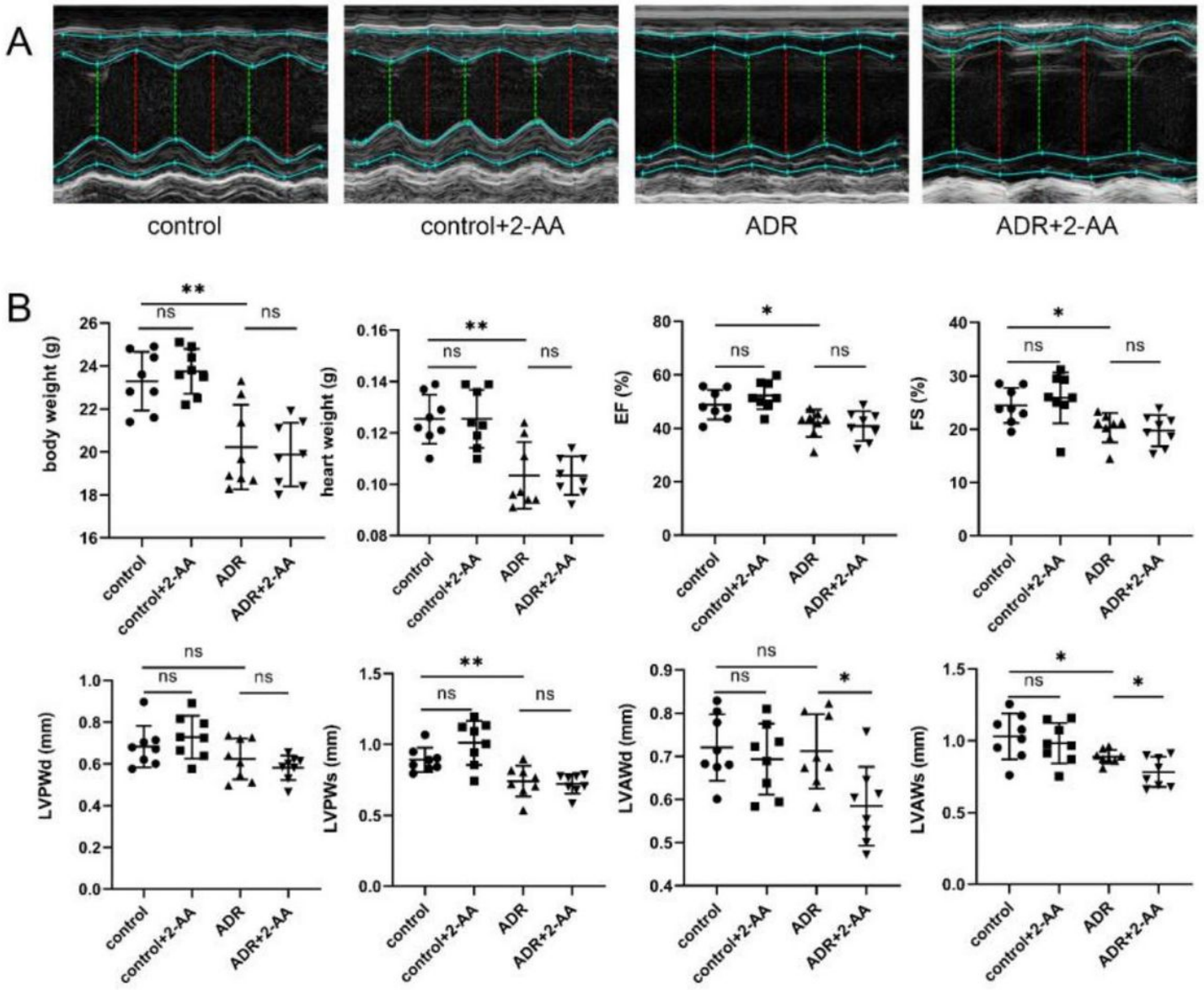


## Figure 3

Effects of L-2-aminoadipic acid (2-AA) on cardiac function in mice with anthracycline-induced cardiotoxicity. (A) Cardiac function and structure were detected by echocardiography, and representative images are presented (n = 8 per group). (B) Body weight, heart weight, ejection fraction (EF%), fractional shortening (FS%), left ventricular anterior wall thickness at end diastole (LVAWd) and systole (LVAWs), and left ventricular posterior wall thickness at end diastole (LVPWd) and systole (LVPWs) were analyzed. Data are presented as the mean ± SD. **$p < 0.01$, *$p < 0.05$, ns = no significant, n = 8 per group.

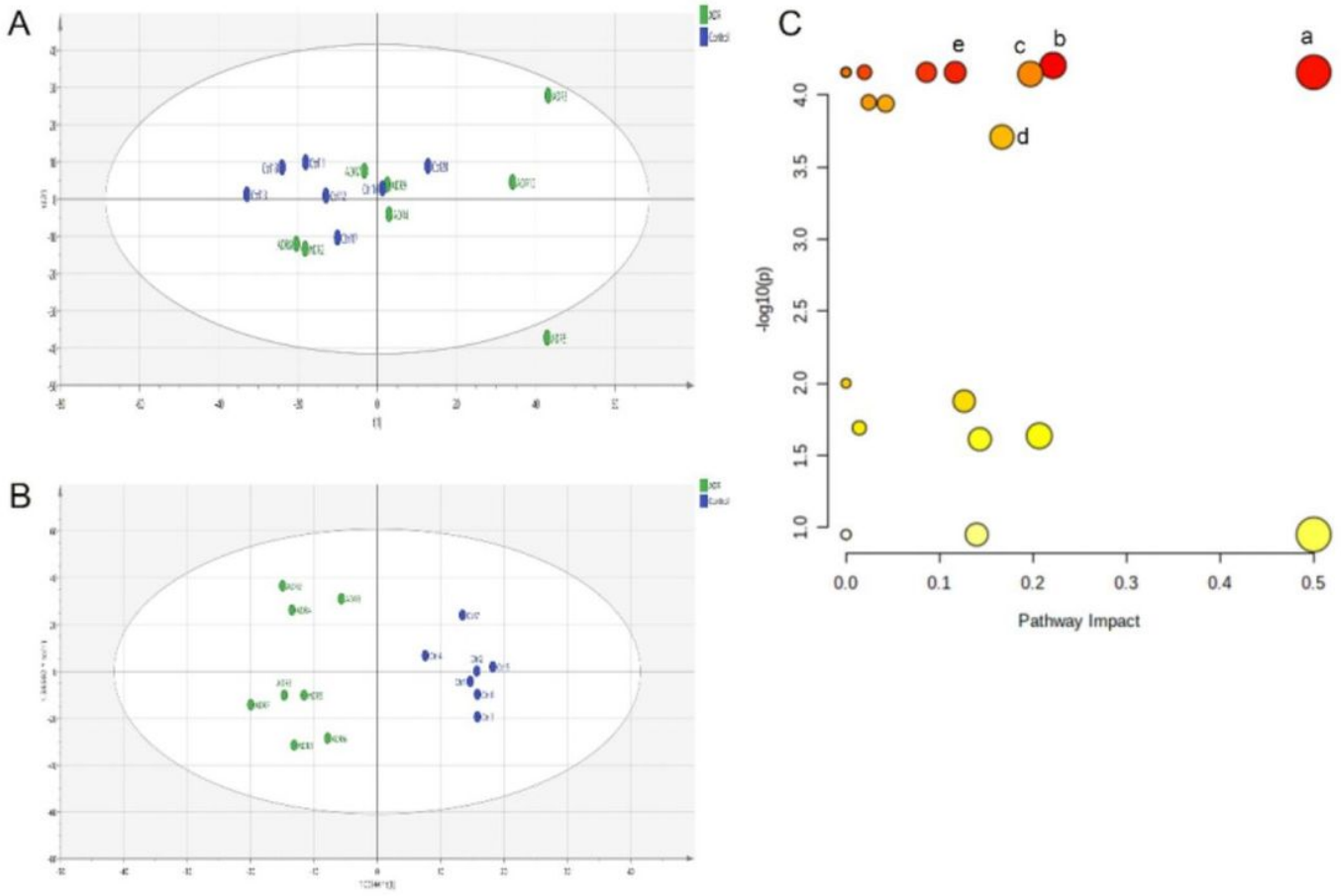


## Figure 4

Amino acid (AA) metabolic signature in mice. (A) Principal component analysis was performed using 51 metabolites from the serum samples. The first two principal components (PCs) explained 68.2% of the total variance (PC1 = 49.9%, PC2 = 18.3%). (B) An orthogonal partial least squares discriminant analysis (OPLS-DA) model was created to analysis the mouse model. The score plot of the OPLS-DA model presented (R2X [cum] = 0.742, R2Y [cum] = 0.931, Q2 = 0.776). The coefficient variability analysis of variance p value for the OPLS-DA model was 0.025. The supervised model was validated by a permutation test (N = 200, Fig. S1A). (C) Metabolic pathway analysis of differential metabolites (a, D-glutamine and D-glutamate metabolism; b, histidine metabolism; c, alanine, aspartate, and glutamate metabolism; d, aminoacyl-tRNA biosynthesis; e. arginine biosynthesis).

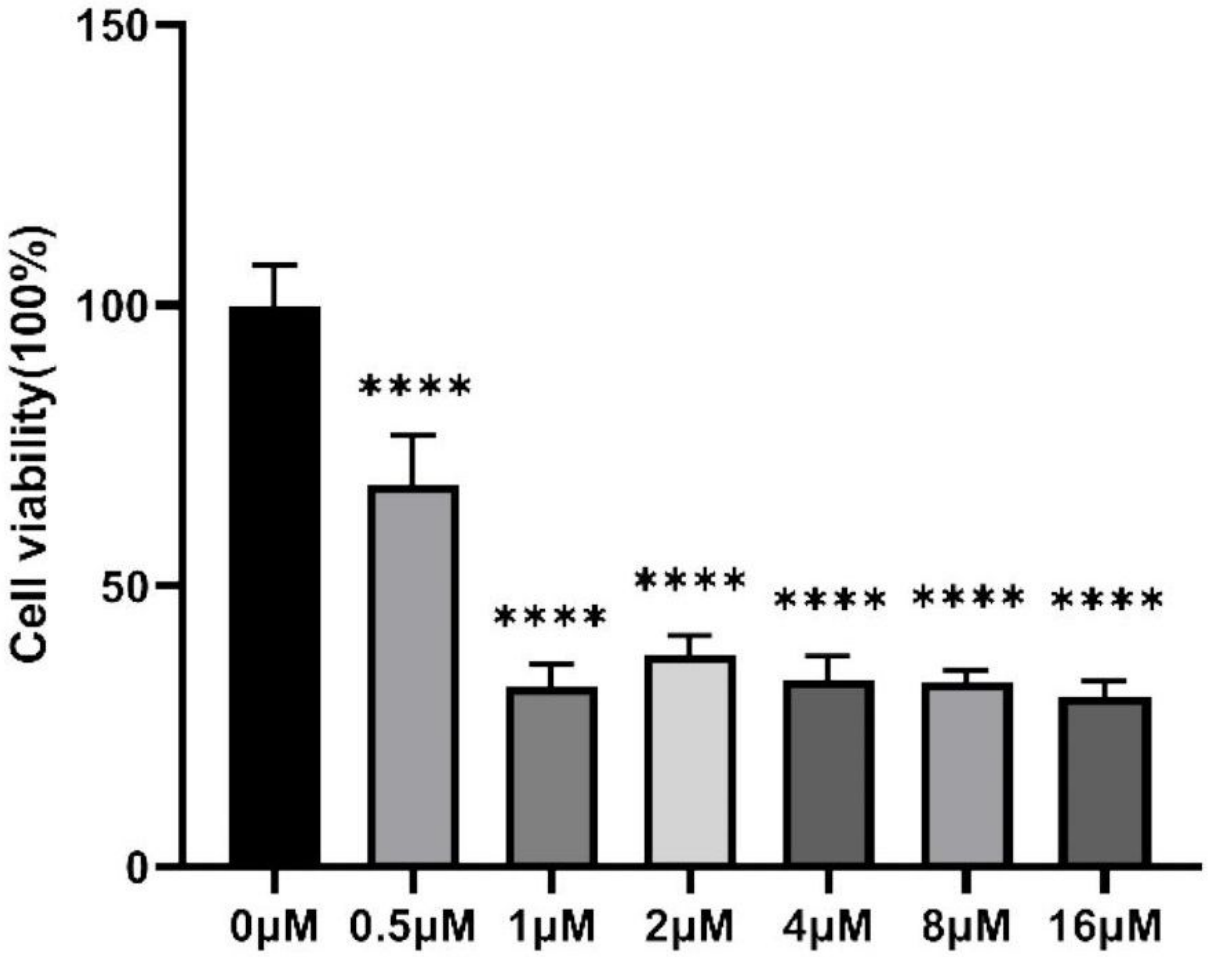


## Figure 5

Adriamycin (ADR) decreases H9c2 cell viability. H9c2 cells were treated with a range of ADR concentrations for 24 h. Cell viability was determined using the Cell Counting Kit-8 assay. Data are presented as the mean ± SD, ****$p < 0.0001$ vs. 0 μM, n = 6 per group.

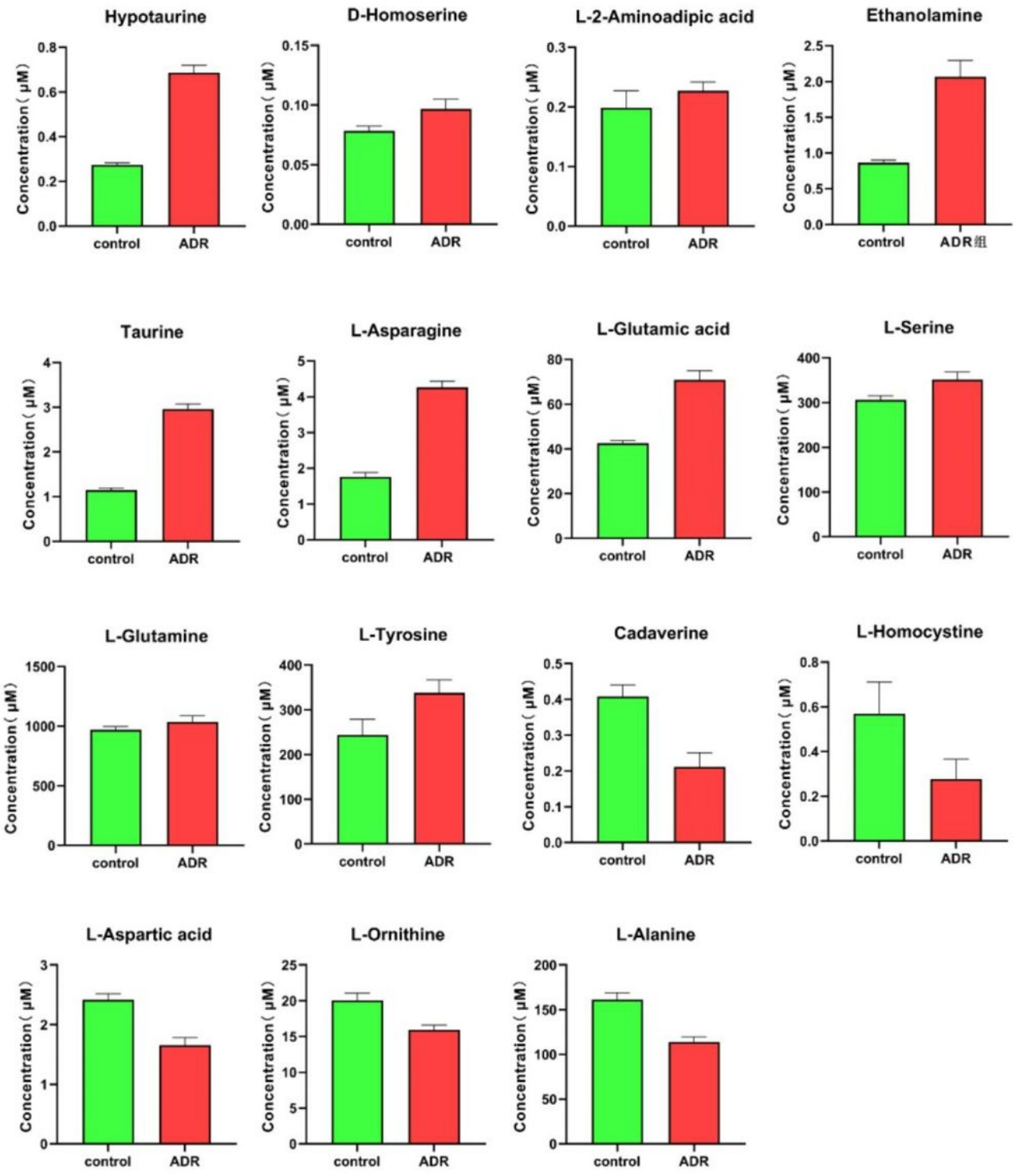


## Figure 6

The concentrations of 15 amino acid (AA) metabolites were changed in the H9c2 cell conditioned medium. The levels of hypotaurine, D-homoserine, L-2-aminoadipic acid, ethanolamine, taurine, L-asparagine, L-glutamic acid, L-serine, L-glutamine, and L-tyrosine were increased in the ADR group, whereas those of cadaverine, L-homocystine, L-aspartic acid, L-ornithine, and L-alanine were decreased.

Data are presented as the mean ± SD, and 15 AA metabolites were significantly different at $p < 0.05$ between the ADR and control groups (n = 6 per group).

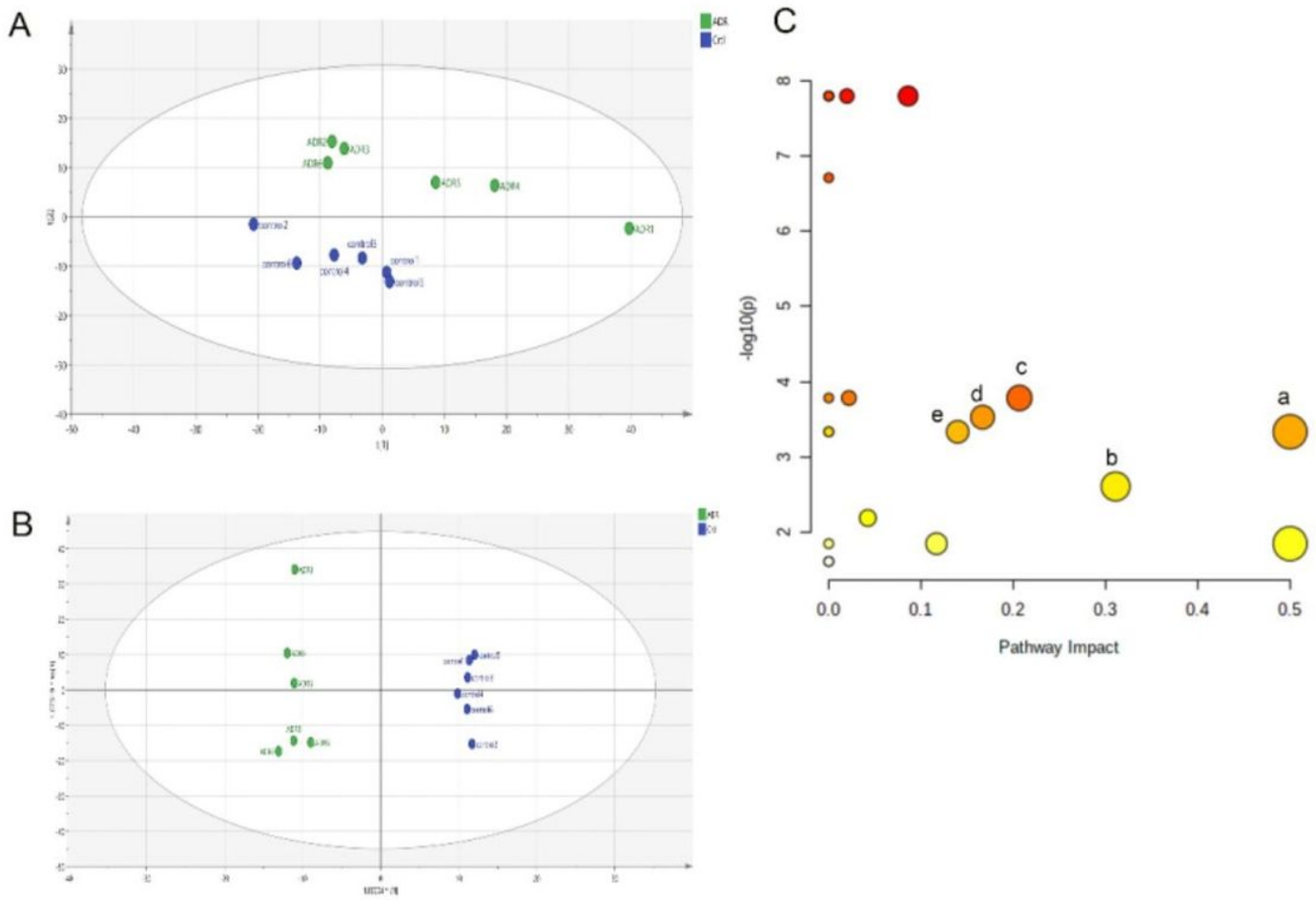


## Figure 7

Amino acid (AA) metabolic signature in the in vitro models. (A) Principal component analysis was performed using 44 metabolites from the conditioned medium samples. The first two principal components (PCs) explained 85.1% of the total variance (PC1 = 60.5%, PC2 = 24.6%). (B) Orthogonal partial least squares discriminant analysis (OPLS-DA) was performed to analyze the in vitro model. The score plot of the OPLS-DA model is presented (R2X [cum] = 0.877, R2Y [cum] = 0.992, Q2 = 0.98). The coefficient variability analysis of variance p value for the OPLS-DA model was 4.97356 × 10−5. The supervised model was validated by a permutation test (N = 200, presented in Fig. S1B). (C) Metabolic pathway analysis of differential metabolites (a, phenylalanine, tyrosine, and tryptophan biosynthesis; b, alanine, aspartate, and glutamate metabolism; c, glycine, serine, and threonine metabolism; d, aminoacyl-tRNA biosynthesis; e, tyrosine metabolism).

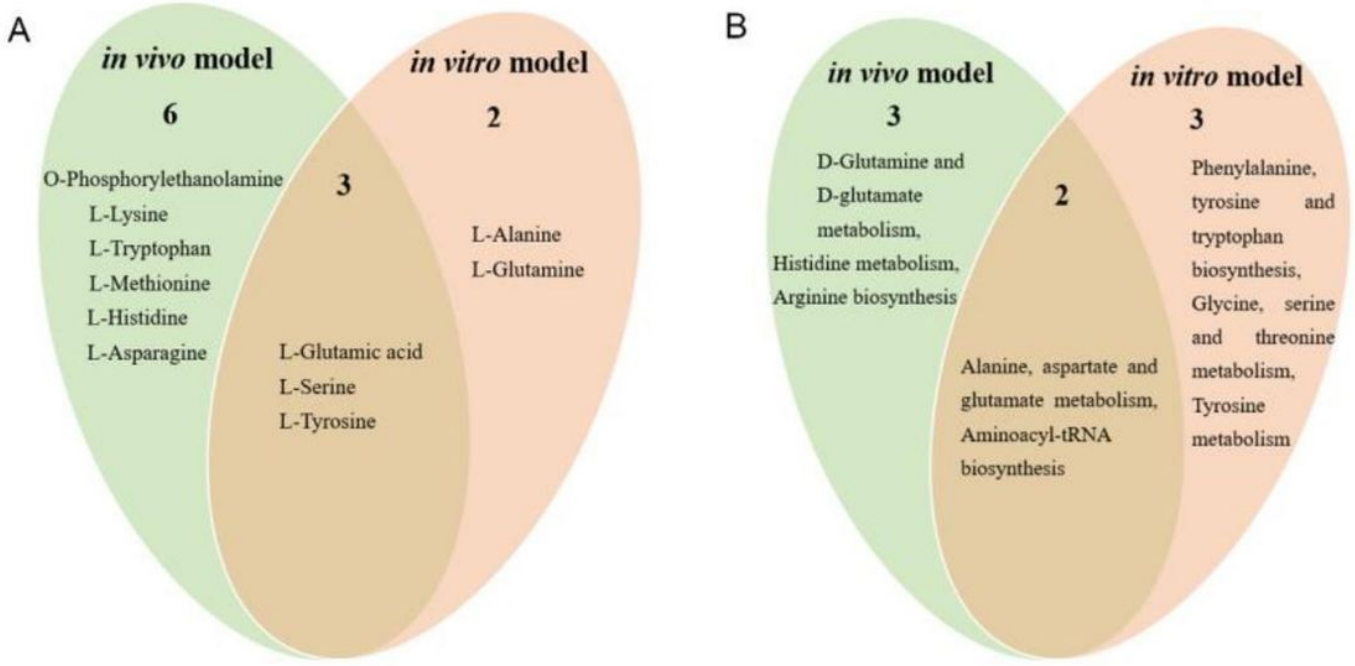


**Figure 8**

Overlap analysis between the in vivo and in vitro models (A) Venn diagram of differential metabolites screened in the two models. (B) Venn diagram of amino acid metabolic pathways screened in the two models. The numbers in the figure represent the same metabolites between the corresponding two models.

## Supplementary Files

This is a list of supplementary files associated with this preprint. Click to download.

- Additionalfile.docx